Issues associated with Galilean invariance on a moving solid boundary in the lattice Boltzmann method

Cheng Peng,[1] Nicholas Geneva,[1] Zhaoli Guo,[2] and Lian-Ping Wang[1,2]
[1]*Department of Mechanical Engineering, University of Delaware, Newark, Delaware 19716-3140, USA*
[2]*State Key Laboratory of Coal Combustion, Huazhong University of Science and Technology, Wuhan, People's Republic of China*
(Received 4 August 2016; revised manuscript received 30 October 2016; published 3 January 2017)

In lattice Boltzmann simulations involving moving solid boundaries, the momentum exchange between the solid and fluid phases was recently found to be not fully consistent with the principle of local Galilean invariance (GI) when the bounce-back schemes (BBS) and the momentum exchange method (MEM) are used. In the past, this inconsistency was resolved by introducing modified MEM schemes so that the overall moving-boundary algorithm could be more consistent with GI. However, in this paper we argue that the true origin of this violation of Galilean invariance (VGI) in the presence of a moving solid-fluid interface is due to the BBS itself, as the VGI error not only exists in the hydrodynamic force acting on the solid phase, but also in the boundary force exerted on the fluid phase, according to Newton's Third Law. The latter, however, has so far gone unnoticed in previously proposed modified MEM schemes. Based on this argument, we conclude that the previous modifications to the momentum exchange method are incomplete solutions to the VGI error in the lattice Boltzmann method (LBM). An implicit remedy to the VGI error in the LBM and its limitation is then revealed. To address the VGI error for a case when this implicit remedy does not exist, a bounce-back scheme based on coordinate transformation is proposed. Numerical tests in both laminar and turbulent flows show that the proposed scheme can effectively eliminate the errors associated with the usual bounce-back implementations on a no-slip solid boundary, and it can maintain an accurate momentum exchange calculation with minimal computational overhead.

DOI: 10.1103/PhysRevE.95.013301

I. INTRODUCTION

In the past 30 years, the lattice Boltzmann method (LBM) has been developed into a viable alternative for solving the Navier-Stokes (NS) equations governing viscous fluid flows. An important reason for its popularity is its apparent simplicity in handling the no-slip boundary condition within complex geometries, which makes it extremely suitable in simulating particle-laden flows [1–4] and flows through porous media [5–7]. In such simulations, the no-slip boundary condition on moving or fixed (typically curved) solid surfaces is usually realized by a bounce-back scheme, which was first proposed in a simple direct bounce-back form [1] and was later modified to achieve at least second-order accuracy on curved boundaries [5,6,8,9]. Also inherited from the gas kinetic theory, the hydrodynamic force acting on a solid body in a LBM simulation can be evaluated by summing the net momentum change between the incident and reflected fluid particles at the boundary nodes during the bounce-back process. This mesoscopic treatment is known as the momentum exchange method (MEM) [1,10]. It is computationally more efficient than its macroscopic counterpart, namely the stress integration method (SIM), as demonstrated in [10,11].

While bounce-back schemes together with the MEM allow different complex geometries to be implemented in the LBM, the existence of a potential violation of Galilean invariance (VGI) in these methods has been exposed both theoretically and numerically [12–16]. By VGI error, we mean that the physical result of the flow, such as the momentum exchange between solid and fluid phases, could change if a constant translational velocity is added to the entire system. Although it is well known that Galilean-invariant NS equations can be derived from the LBM scheme via different methods, e.g., Chapman-Enskog analysis [17], asymptotic expansion [18,19], or linear analysis [20], these derivations often do not consider the presence of a solid boundary. In the LBM, popular solid boundary schemes can be roughly grouped into two categories: (i) constructing the mesoscopic distribution functions at the boundary by, e.g., bounce-back rules [1,5,6,8,9] and by directly formulating from the local fluid pressure, velocity, and stress information [21]; and (ii) satisfying the boundary constraints at the level of macroscopic or NS equations [e.g., the immersed boundary method (IBM)] [22,23]. For example, the hydrodynamic forces in IBM-LBM are evaluated according to the NS equations on a set of Lagrangian points attached to the solid surfaces [22,23]. Such forces are then inverted and interpolated as an effective body force exerted on the fluid phase. Thus, in the second category, Galilean invariance is expected to be preserved, and we will no longer consider this category in our paper.

In past studies [12–16], the VGI error was attributed to the MEM. Therefore, in order to correct the VGI error associated with the treatment of a moving solid boundary, several different modifications of the MEM have been proposed to improve or restore Galilean invariance (GI) in the calculation of hydrodynamic force acting on a solid boundary. To our knowledge, Caiazzo and Junk [12] were among the first to realize the lack of Galilean invariance in the MEM, and they proposed a corrected MEM by subtracting the linkwise VGI error directly on each link. Such linkwise correction is a brute-force treatment that ensures the error will be eliminated on all boundary links. Later, Clausen and Aidun [13] presented a straightforward correction that acts in a nodewise manner for an arbitrarily orientated surface. The nodewise correction is designed to remove the overall VGI error on each boundary node. Compared to the linkwise treatment, the major issue for such nodewise correction is

that its performance may be affected by the boundary link configuration. Another problem for both correction methods is that they require the VGI errors to be formulated and calculated beforehand so that the precise errors can be subtracted in their algorithms. Such calculations of VGI errors involve certain assumptions (e.g., the system is fully relaxed), and they are independent of the flow around, so these corrections may not be accurate. Chen *et al.* [14] proposed a corrected MEM to incorporate the impulsive force [2] when a solid node becomes a fluid node, or *vice versa*. Although it was not intended to eliminate VGI error, their treatment was later interpreted as a linkwise correction that essentially achieves similar nodewise correction in certain ideal cases [24]. More recently, Wen *et al.* designed a Galilean-invariant momentum exchange method (GIMEM) in which the lattice fluid velocity relative to the wall was used to realize nodewise Galilean invariance [15]. Compared with its alternatives, this formulation does not require explicit computation of the VGI error. Since its correction term depends on flow information, i.e., boundary distribution functions, this method could potentially work better under insufficient grid resolutions. A similar correction was proposed by Krithivasan *et al.* [16] around the same time. Numerical simulations of both laminar and turbulent particle-laden flows indicate that the above-mentioned corrected force evaluation schemes in Refs. [12–15] lead to physically correct solid-particle motions [15,24,25]. Further details on these methods are discussed in Wen *et al.*'s review article [26].

In this paper, we argue that all the above-mentioned modifications shall not be considered as complete solutions to the VGI errors in the LBM. Their incompleteness can be easily seen by considering Newton's Third Law. Namely, if there exists a VGI error in the hydrodynamic force acting on the solid phase, there must be a corresponding VGI error in terms of interaction force experienced by the fluid phase, with the latter being equal and opposite to the former. However, the latter issue remains essentially unnoticed by all the proposed corrections since none of them changes the core algorithm of the LBM, i.e., the evolution of distribution functions near a moving fluid-solid interface. The amount of momentum change in the fluid phase due to the moving solid boundary in the LBM is purely determined by the bounce-back process, which is left unchanged no matter what postprocessing modifications are made to the momentum exchange scheme. In other words, the focus of these modifications is on the evaluation of the hydrodynamic force and torque acting on the solid phase, but ignoring the feedback effect of the fluid phase. Without fixing the VGI error on the fluid phase, the one-way correction on the hydrodynamic force evaluation can lead to the violation of Newton's Third Law. In this regard, the previous modifications to the MEM are flawed. We will discuss this issue in detail in Sec. II.

We will reveal in detail later in this paper, for some cases, that the VGI error on the fluid may be corrected impulsively through momentum gain or loss when a given lattice node switches phase, i.e., a fluid node becomes a solid node or *vice versa*. However, in some other cases in which this impulsive fix does not occur, e.g., the case in which the wall moves along a fixed line (in two dimensions) or surface (in three dimensions) relative to the fixed lattice nodes, the VGI error on the fluid phase is left uncorrected. For such specific situations, the existing bounce-back schemes need to be improved to address this issue, which is the main focus of this paper.

The rest of this paper is arranged as follows. In Sec. II, we first demonstrate that the true origin of VGI error lies in the bounce-back scheme (the core algorithm) instead of the momentum exchange method (the postprocessing part). Based on this argument, we briefly introduce the previous modified momentum exchange schemes and assess their incompleteness both theoretically and numerically. An implicit remedy to the VGI error in the LBM and its limitations are then revealed. To eliminate the VGI error in the absence of such a remedy, a boundary scheme is presented that will restore GI for both fluid and solid phases. The proposed scheme is validated in Sec. IV using a Poiseuille flow between two inclined walls, a turbulent channel flow, and a turbulent pipe flow. Finally, the contents of this work are highlighted in Sec. V with a summary of key conclusions.

II. ANALYSIS OF DEVIATIONS FROM THE GALILEAN INVARIANCE IN THE LBM

In the LBM, the mesoscopic fluid-particle distribution function $f_i(\mathbf{x},t)$ is governed by

$$f_i(\mathbf{x}+\mathbf{e}_i,t+\delta_t)-f_i(\mathbf{x},t)=\Omega_i, \tag{1}$$

where i refers to a discrete particle velocity $\mathbf{e}_i$, $\mathbf{x}$ and t are the discrete node and time, respectively, and δ_t is the time step size. The right-hand side (RHS) of Eq. (1) is the collision operator, which can take different forms depending on the specific collision model being chosen. The first typical collision model is the single-relaxation-time [or Bhatnagar-Gross-Krook (BGK)] model

$$\Omega_i=-\frac{1}{\tau}\left[f_i(\mathbf{x},t)-f_i^{(\mathrm{eq})}(\mathbf{x},t)\right], \tag{2}$$

where τ is a nondimensional relaxation time that is related to the kinematic viscosity ν as $\nu=c_s^2(\tau-0.5)\delta_t$ (where c_s is the model speed of sound), and $f_i^{(\mathrm{eq})}$ is the corresponding equilibrium distribution function. The second commonly used collision model is the multi-relaxation time (MRT) model

$$\Omega_i=-\mathbf{M}^{-1}\mathbf{S}\mathbf{M}\left[f_i(\mathbf{x},t)-f_i^{(\mathrm{eq})}(\mathbf{x},t)\right], \tag{3}$$

where $\mathbf{M}$ and $\mathbf{M}^{-1}$ are the transform matrix and its inverse, respectively, that relate the distribution functions with the same number of independent moments. $\mathbf{S}$ is the diagonal matrix that defines the relaxation coefficient of each moment. The macroscopic (continuum) density and fluid momentum are obtained in terms of the zeroth- and first-order moments of the distribution functions f_i.

A. Momentum exchange between solid and fluid phases

As mentioned in the Introduction, in the past the VGI issue in the LBM was dealt with only partially by modifying the momentum exchange method [12–16]. Such modifications impact the solid phase only, without a corresponding effect on the fluid phase. As we shall see shortly, this one-way change is flawed and incomplete. The true origin of the VGI error lies in the inappropriate construction of the unknown

distribution functions at boundary points near the moving solid-fluid interface, namely the bounce-back scheme itself.

To understand our argument more clearly, let us consider a simple case in which a fluid flow with some initial momenta is present in a pipe. This flow is decelerated due to the wall drag force. In this case, the only force that changes the total momenta of the fluid is the drag force exerted by the wall $\mathbf{F}'$. Based on the principle of Galilean invariance, the fluid inside the pipe should decelerate at the same rate regardless of the frame of reference used. The total momentum change of the fluid phase between t and $t+\delta_t$ can be formulated as

$$\mathbf{m}(t+\delta_t)-\mathbf{m}(t)=\mathbf{F}'\delta_t. \tag{4}$$

In the LBM, the fluid momenta $\mathbf{m}$ are calculated as

$$\mathbf{m}(t+\delta_t)=\sum_{\mathbf{x},i} f_i(t+\delta_t)\mathbf{e}_i, \quad \mathbf{m}(t)=\sum_{\mathbf{x},i} f_i(t)\mathbf{e}_i, \tag{5}$$

where the above summations are over all the lattice directions i and all the fluid node points $\mathbf{x}$ in the volume considered.

When the external body force or mean pressure gradient is absent, we have the following relationship between postcollision and precollision fluid momenta:

$$\sum_{\mathbf{x},i} f_i(t)\mathbf{e}_i=\sum_{\mathbf{x},i} f_i^*(t)\mathbf{e}_i, \tag{6}$$

where $f_i(t)$ and $f_i^*(t)$ are the pre- and postcollision distribution functions at a given time step.

Substitute Eqs. (5) and (6) into Eq. (4), we have

$$\mathbf{F}'\delta_t=\sum_{\mathbf{x},i} f_i(t+\delta_t)\mathbf{e}_i-\sum_{\mathbf{x},i} f_i^*(t)\mathbf{e}_i. \tag{7}$$

If we consider the fluid phase as a whole, we note that the inner propagation (or streaming) between two fluid nodes does not change the total momenta of the fluid. The only contribution to the fluid momentum change is governed by the fluid particles incident and reflected off the solid boundary. Therefore, Eq. (7) can be rewritten as

$$\begin{aligned}\mathbf{F}'\delta_t &= \sum_{\text{Blinks}} [f_{\bar{i}}(t+\delta_t)\mathbf{e}_{\bar{i}}-f_i^*(t)\mathbf{e}_i] \\ &= -\sum_{\text{Blinks}} [f_{\bar{i}}(t+\delta_t)+f_i^*(t)]\mathbf{e}_i,\end{aligned} \tag{8}$$

where $f_{\bar{i}}(t+\delta_t)\mathbf{e}_{\bar{i}}$ represents the momenta carried by the fluid particles coming from the solid phase, and $f_i^*(t)\mathbf{e}_i$ is the momenta carried by the fluid particles entering the solid phase.

It should be noted that Eq. (8) is a general fact in the LBM that does not change regardless of the algorithm one uses to evaluate the hydrodynamic force acting on the solid phase. In fact, to satisfy Newton's Third Law, the force exerted on the fluid phase must be precisely opposite to the hydrodynamic force $\mathbf{F}$ acting on the solid phase, which leads to

$$\mathbf{F}\delta_t=-\mathbf{F}'\delta_t=\sum_{\text{Blinks}} [f_{\bar{i}}(t+\delta_t)+f_i^*(t)]\mathbf{e}_i. \tag{9}$$

As we shall realize soon, Eq. (9) is simply the summation form of the conventional MEM, which accurately describes the momentum exchange between solid and fluid phases. Clearly, we have identified *a fundamental inconsistency* in all the previous studies that modify the conventional MEM in order to restore Galilean invariance, which motivated the current study.

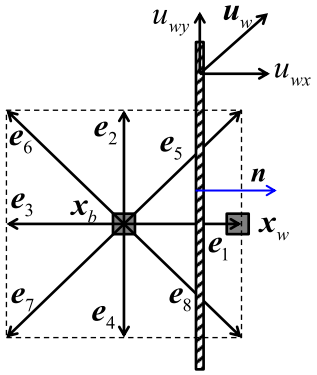

FIG. 1. Configuration of a boundary node that interacts with a moving wall.

B. The VGI error in the momentum exchange

In this subsection, we shall discuss the Galilean variant issue of momentum exchange between solid and fluid phases and reveal its true origin. Consider a moving solid wall and a lattice node ($\mathbf{x}_b$) next to the solid wall in the fluid domain, as illustrated in Fig. 1. There are several fluid lattice particles sitting at $\mathbf{x}_b$ that will travel along the boundary links. These lattice particles interact with the solid boundary causing momentum exchanges between the solid boundary and the fluid. The net momentum exchange between this fluid node and the wall should be identical whether the whole system is at rest or moving with a constant velocity. This is the principle of Galilean invariance. This fundamental principle must be preserved in any nonaccelerating inertial frame of reference.

As we discussed before, the momentum exchange between the fluid at the boundary node point $\mathbf{x}_b$ and the solid wall must be

$$\begin{aligned}\mathbf{F}(\mathbf{x}_b)\delta_t &= -\mathbf{F}'(\mathbf{x}_b)\delta_t=\sum_{\text{Blinks}} [f_{\bar{i}}(t+\delta_t)+f_i^*(t)]\mathbf{e}_i \\ &= \sum_{i=1,5,8} [f_{\bar{i}}(t+\delta_t)+f_i^*(t)]\mathbf{e}_i.\end{aligned} \tag{10}$$

Here we use the notation $\mathbf{F}(\mathbf{x}_b)\delta_t$ to indicate the momentum change of the solid phase, and $\mathbf{F}'(\mathbf{x}_b)\delta_t$ for the momentum change of the fluid phase. Typically, in the bounce-back scheme they are related by

$$f_{\bar{i}}(t+\delta_t)=f_i^*(t)-\frac{2w_i\rho_0}{c_s^2}(\mathbf{e}_i\cdot\mathbf{u}_w), \tag{11}$$

where $\mathbf{u}_w$ is the velocity of the solid boundary and w_i is the weighting factor. Here, the incompressible formulation of He and Luo [27] has been adopted, namely the density is decomposed into a mean reference density ρ_0 and a local fluctuation $\delta\rho$. The second term on the RHS in the above equation approximates the no-slip boundary condition on a moving wall.

In a "fully relaxed system," in which the whole flow field is at the same state (i.e., velocity, temperature, etc.) as the solid boundary, we can represent both f_i^* and $f_{\bar{i}}$ with their

corresponding equilibrium distributions in terms of the local density fluctuation $\delta\rho$ and velocity $\mathbf{u}_w$ at the wall,

$$f_i^{(\mathrm{eq})} = w_i\delta\rho + \rho_0 w_i\left[\frac{(\mathbf{e}_i\cdot\mathbf{u}_w)}{c_s^2} + \frac{(\mathbf{e}_i\cdot\mathbf{u}_w)^2}{2c_s^4} - \frac{(\mathbf{u}_w\cdot\mathbf{u}_w)}{2c_s^2}\right]. \tag{12}$$

Substituting the equilibrium distribution into the MEM equation, Eq. (9), one can express the momentum exchange as

$$\mathbf{F}(\mathbf{x}_b)\delta_t = \sum_{\text{Blinks}}\left\{2w_i\mathbf{e}_i\delta\rho + \rho_0 w_i\mathbf{e}_i\left[\frac{(\mathbf{e}_i\cdot\mathbf{u}_w)^2}{c_s^4} - \frac{(\mathbf{u}_w\cdot\mathbf{u}_w)}{c_s^2}\right]\right\}. \tag{13}$$

Assuming a D2Q9 lattice grid and summing over all boundary links in the case of Fig. 1 results in the nodewise momentum exchange as

$$\mathbf{F}(\mathbf{x}_b)\delta_t = \frac{1}{3}\delta\rho c\mathbf{n} + \frac{\rho_0}{c}u_{wx}\mathbf{u}_w \approx \frac{1}{3}\delta\rho c\mathbf{n} + \frac{\rho_0}{c}(\mathbf{u}_w\cdot\mathbf{n})\mathbf{u}_w, \tag{14}$$

where $\mathbf{n}$ is the unit wall normal vector [$\mathbf{n} = (1,0)$ in this case] pointing from the boundary fluid node $\mathbf{x}_b$ to the wall surface. The first term on the RHS of Eq. (14) is precisely the hydrodynamic force due to the fluid pressure ($p\mathbf{n}$). Since the system is in a fully relaxed state, this should be the only force acting on the solid boundary. Therefore, the second term on the RHS of Eq. (14), which depends on the wall velocity magnitude u_{wx} and u_{wy}, represents the VGI error in force evaluation, namely,

$$\mathbf{F}_{\mathrm{VGI}}(\mathbf{x}_b)\delta_t = \frac{\rho_0}{c}(\mathbf{u}_w\cdot\mathbf{n})\mathbf{u}_w. \tag{15}$$

It should be noted that the last expression in Eq. (14) is approximate as, due to the discretization and lattice grid layout, the intermediate expression remains correct even if the local wall normal deviates slightly from the horizontal direction. Again, it is necessary to emphasize that Eq. (13) is the actual momentum exchange between the fluid at boundary $\mathbf{x}_b$ and the solid wall, which is independent of the scheme that is used to evaluate it. The VGI error exists in both the hydrodynamic force acting on the solid wall as well as the reaction force exerted on the fluid phase. However, in previous studies [12,13,15], the latter was not realized. The efforts to date have been focused on modifying the force evaluation scheme to enforce the Galilean invariance of the former only. These corrections are thus part of the postprocessing, instead of eliminating the VGI error from its true origin. As one could observe in Eq. (9), the only flexibility that can be taken advantage of to restore Galilean invariance in the momentum exchange between phases is the distribution function $f_{\bar{i}}(t+\delta_t)$ being constructed via the boundary schemes. Therefore, better bounce-back schemes need to be proposed to resolve this issue fully.

C. Modified momentum exchange methods

For the completeness of our discussion, we shall first review the previous efforts to address the VGI errors, i.e., the improved momentum exchange schemes proposed in Refs. [12–15]. Among these efforts, the schemes of Caiazzo and Junk [12], Clausen and Aidun [13], and Chen *et al.* [14] all require direct computation of the VGI error in terms of distributions under the fully relaxed assumption, so they are discussed together.

Since the momentum exchange between solid and fluid phases should be independent of the wall reference velocity, the velocity-dependent part in Eq. (9) should be viewed as a source for the VGI error, and it shall be offset in the calculation of hydrodynamic force acting on the solid wall. Starting from that point, Caiazzo and Junk [12] proposed a corrected momentum exchange algorithm by directly subtracting the velocity-dependent part from the momentum exchange to enforce GI on each boundary link, as

$$\mathbf{F}(\mathbf{x}_b)\delta_t = \sum_{\text{Blinks}}\left\{[f_{\bar{i}}(t+\delta_t) + f_i^*(t)]\mathbf{e}_i - \rho_0 w_i\mathbf{e}_i \times\left[\frac{(\mathbf{e}_i\cdot\mathbf{u}_w)^2}{c_s^4} - \frac{(\mathbf{u}_w\cdot\mathbf{u}_w)}{c_s^2}\right]\right\}. \tag{16}$$

This correction is straightforward to implement. Since GI is enforced on each link, the force evaluation at each node point is expected to have the same property, regardless of the boundary link configuration.

Different from Caiazzo and Junk, Clausen and Aidun [13] designed a modified MEM by correcting the VGI error in the force evaluation in a nodewise manner. In Ref. [13], the nodewise VGI error in Eq. (15) is simply subtracted from the actual momentum exchange, i.e., Eq. (9), to restore Galilean invariance. When the wall is arbitrarily oriented, with $\mathbf{n} = (n_x,n_y)$, where $\mathbf{n}$ is the unit wall normal vector pointing from the boundary fluid node $\mathbf{x}_b$ to the wall surface, the momentum exchange evaluated by Clausen and Aidun's modified scheme can be approximated as

$$\mathbf{F}(\mathbf{x}_b)\delta_t = \sum_{\text{Blinks}}(f_i^* + f_{\bar{i}})\mathbf{e}_i - \frac{\rho_0}{c}(\mathbf{u}_w\cdot\mathbf{n})\mathbf{u}_w. \tag{17}$$

It should be noted that in the original formulation proposed by Clausen and Aidun, the term $\delta\rho c\mathbf{n}/3$ in Eq. (14) was also treated as part of the VGI error. However, this term clearly represents the pressure's contribution in the momentum exchange, which can be nonzero even if the fluid at $\mathbf{x}_b$ is stationary relative to the wall. Thus, in this paper, this term is not considered as part of the VGI error, contrary to Clausen and Aidun's original proposal.

Alternatively, Chen *et al.* [14] pointed out that there existed a nonzero fluid mass being displaced by the moving fluid-solid interface in Eq. (11). This displaced fluid mass contains momenta that are ignored in the conventional MEM. Therefore, they corrected the momentum exchange calculation as

$$\begin{aligned}\mathbf{F}(\mathbf{x}_b)\delta_t &= \sum_{\text{Blinks}}\left[(f_i^* + f_{\bar{i}})\mathbf{e}_i - \frac{2w_i\rho_0}{c_s^2}(\mathbf{e}_i\cdot\mathbf{u}_w)\mathbf{u}_w\right] \\ &= \sum_{\text{Blinks}}(f_i^* + f_{\bar{i}})\mathbf{e}_i - \frac{\rho_0}{c}\mathbf{u}_w\sum_{\text{Blinks}}6w_i\left(\frac{\mathbf{e}_i}{c}\cdot\mathbf{u}_w\right),\end{aligned}$$

where the last term represents the momentum exchange contributed by the displaced fluid mass. It is noted that Chen *et al.*'s method is a linkwise correction. The total amount of correction depends on the boundary link configuration, and the last summation in Eq. (18) generally cannot be converted to

the form in Eq. (17) or Eq. (16). However, in some ideal cases, for example a horizontal or a vertical wall, Eqs. (16), (17), and (18) become identical. Nevertheless, the correction terms in the above three schemes are very similar in form, and they have no dependence on the local flow, i.e., the distribution functions, rather they are determined solely by the state of the solid phase (and the boundary link configuration in the case of Chen *et al.*). These schemes also require explicit computation of the VGI error under the assumption of a fully relaxed system and a simple bounce-back rule, i.e., bounce-back without interpolation, which could potentially contain numerical errors when an *interpolated* bounce-back scheme is used.

In Ref. [15], a Galilean invariant momentum exchange method (GIMEM) is introduced, and the momentum exchange is computed instead as

$$\mathbf{F}(\mathbf{x}_b)\delta_t = \sum_{\text{Blinks}} [f_i^*(\mathbf{e}_i - \mathbf{u}_w) - f_{\bar{i}}(\mathbf{e}_{\bar{i}} - \mathbf{u}_w)]. \tag{18}$$

This scheme follows a simple physical principle that the momentum exchange between two objects should be expressed based on their relative velocity, in this case between the fluid lattice particle and the solid boundary, as opposed to the absolute velocity of the lattice particle. Contrary to the schemes in Refs. [12–14], the correction term in this method is related to the actual value of both incident and bounce-back populations. Thus the method by Wen *et al.* is arguably more compatible when an *interpolated* bounce-back scheme is used.

We can also compare the correction terms in the above four methods in the limiting case of a fully relaxed state in Fig. 1. It is easy to prove the following identities:

$$\begin{aligned}
&\mathbf{u}_w \sum_{i=1,5,8} (-f_i^* + f_{\bar{i}}) \\
&= \mathbf{u}_w \sum_{i=1,5,8} \left[- f_i^{(\text{eq})} + f_{\bar{i}}^{(\text{eq})} \right] \\
&= -\mathbf{u}_w \frac{\rho_0}{c} (\mathbf{u}_w \cdot \mathbf{n}) \\
&= -\frac{\rho_0}{c} \mathbf{u}_w \sum_{i=1,5,8} 6 w_i \left(\frac{\mathbf{e}_i}{c} \cdot \mathbf{u}_w \right) \\
&= -\sum_{i=1,5,8} \left\{ \rho_0 w_i \mathbf{e}_i \left[\frac{(\mathbf{e}_i \cdot \mathbf{u}_w)^2}{c_s^4} - \frac{(\mathbf{u}_w \cdot \mathbf{u}_w)}{c_s^2} \right] \right\}.
\end{aligned} \tag{19}$$

The above discussions show that the four different corrections in the literature, although not identical, are closely related.

However, regardless of what modifications are made, they do not correct the VGI error in the actual momentum exchange between solid and fluid phases, rather they make the expression of hydrodynamic force acting on the solid phase appear to be Galilean-invariant. Since these modifications only change the force evaluation on the solid phase, they could potentially break Newton's Third Law, as the force they obtain may not be equal to its opposite force exerted on the fluid phase.

D. An implicit remedy of correcting the VGI error in the LBM

In addition to the bounce-back interaction on the fluid-solid surface, the momentum exchange between fluid and solid phases also occurs when a fluid node is covered by a moving solid body or when a solid node is uncovered. We will refer to this process as *node-type switching*. When a fluid node becomes a solid node, all the momentum at this node disappears in the fluid domain, which should be converted as a force acting on the solid phase, and *vice versa*. As we shall see shortly, such impulsive momentum exchange between the two phases can be viewed as a discrete correction to the accumulative VGI errors that take place continuously. To demonstrate this, let us reexamine the case shown in Fig. 1. Recalling Eq. (8), Eq. (15) suggests that there is a VGI error to the fluid phase during each time step, which can be expressed as

$$\mathbf{F}'_{\text{VGI}}\delta_t = -\frac{\rho_0}{c}(\mathbf{u}_w \cdot \mathbf{n})\mathbf{u}_w. \tag{20}$$

Assuming that the wall moves with constant velocity $\mathbf{u}_w$, this correction shall happen in $c/(\mathbf{u}_w \cdot \mathbf{n})$ time steps before the solid node $\mathbf{x}_w$ on the right is uncovered. The VGI error to the fluid momentum in this process accumulates as

$$\mathbf{M}_{\text{VGI,tot}} = \mathbf{F}'_{\text{VGI}}\delta_t \cdot \frac{c}{\mathbf{u}_w \cdot \mathbf{n}} = -\rho_0 \mathbf{u}_w. \tag{21}$$

On the other hand, once the node $\mathbf{x}_w$ changes from a solid to a fluid node, the distribution functions at this node need to be constructed or initialized. Such reconstruction is also known as the refilling process [24,28–30]. Due to the constraint of non-slip boundary condition, the velocity at $\mathbf{x}_w$ is expected to be identical with the wall velocity $\mathbf{u}_w$, so the momentum gain for the fluid phase is

$$\mathbf{M}_{\text{gain}}(\mathbf{x}_w) = \rho_0 \mathbf{u}_w, \tag{22}$$

which cancels precisely with the total VGI error previously accumulated. The same cancellation can be observed when the wall moves in the opposite direction and eventually covers the boundary node $\mathbf{x}_b$.

For the fluid phase, such impulsive correction is carried out naturally with a moving solid boundary with respect to the lattice grid itself, and it provides a self-healing mechanism that maintains the overall Galilean invariance for the fluid phase over a time scale of the order $c\delta_t/(\mathbf{u}_w \cdot \mathbf{n})$. However, since this self-healing mechanism relies on the solid boundary to physically move with respect to the lattice, covering or uncovering specific nodes, its drawback is obvious. For a flow in which the moving solid boundary does not shift relative to the lattice grid and node-type switching is absent, such as the case in which the wall moves along a fixed line (in two dimensions) or surface (in three dimensions) relative to the lattice nodes, the VGI error in the fluid phase resulting from the bounce-back can no longer be naturally fixed. It is worth pointing out that for the configuration in Fig. 1 (i.e., a flat vertical wall), the VGI error is zero when $u_{wx} = 0$, as indicated by Eq. (15). But the VGI error can become nonzero when the wall is either inclined or curved, or when an interpolated bounce-back scheme is needed, as shown by simulation examples below and in Sec. IV.

To explicitly demonstrate the VGI error for the fluid phase, we present a simple numerical test case of a Poiseuille flow between two inclined walls driven by a body force. The flow schematic is shown in Fig. 2. Here we choose to make the channel walls inclined to mimic the more general case of curved boundaries. In the simulations, we set $\theta = \tan^{-1}(1/2)$,

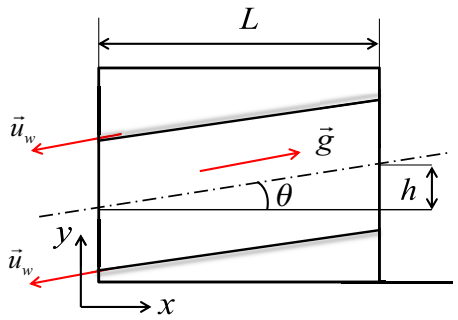

FIG. 2. Sketch of a Poiseuille flow driven by a constant body force between two inclined walls.

$h = 10$, $L = 20$, and the channel width $H = 40$. The fluid is driven by a constant body force to have a centerline velocity $u_c = 0.01$ (relative to the channel walls), in parallel with the channel centerline. The simulation is carried out with a MRT LB model introduced in [20], using the same suggested relaxation parameters for those moments that are irrelevant to the NS equations. The viscosity is chosen as $\nu = 0.02$. Several simulations were performed, with the walls moving in the direction opposite to the flow driving force, with wall velocity magnitude varying from $u_w = 0.05$ to 0.15. To resolve the solid boundaries with second-order accuracy, two popular linear interpolated bounce-back schemes developed by Bouzidi *et al.* [8] and Yu *et al.* [5] are tested. For completeness of our discussion, the same simulation with the simple bounce-back [1] scheme is also presented in parallel. It is noted that, to demonstrate the VGI error on the fluid phase, we purposely introduce a large velocity of the moving frame, relative to the flow velocity change across the channel.

The velocity profiles at the steady state with different wall translation velocities u_w are plotted in Fig. 3. As clearly illustrated in the plots, the velocity profiles with large wall velocity magnitudes deviate significantly from the theoretical results with the two interpolated bounce-back schemes. Such results imply that the VGI error introduces additional wall drag to the fluid phase, which causes a reduction in the steady-state flow speed. Since in this case the solid boundary does not shift with respect to the lattice nodes, the self-healing mechanism previously mentioned is absent, so that the VGI error accumulates, resulting in reduced overall accuracy of the simulation. On the other hand, the velocity profiles with the simple bounce-back scheme do not present significant VGI error, as the profiles with different wall velocities collapse together. When the simple bounce-back scheme is employed, the momentum exchange between solid and fluid phases only depends on the information at the boundary nodes, which makes our idealized analysis in Sec. II B applicable. As implied by Eq. (15), in this situation the VGI error on each link cancels out and results in a negligible error at each boundary node. However, since the simple bounce-back has only first-order accuracy, the numerical error due to insufficient discretization is much larger than the two cases with interpolated bounce-back schemes. Although the simple bounce-back scheme can be viewed as free of VGI error, it is not recommended in the LBM simulations involving complex geometries.

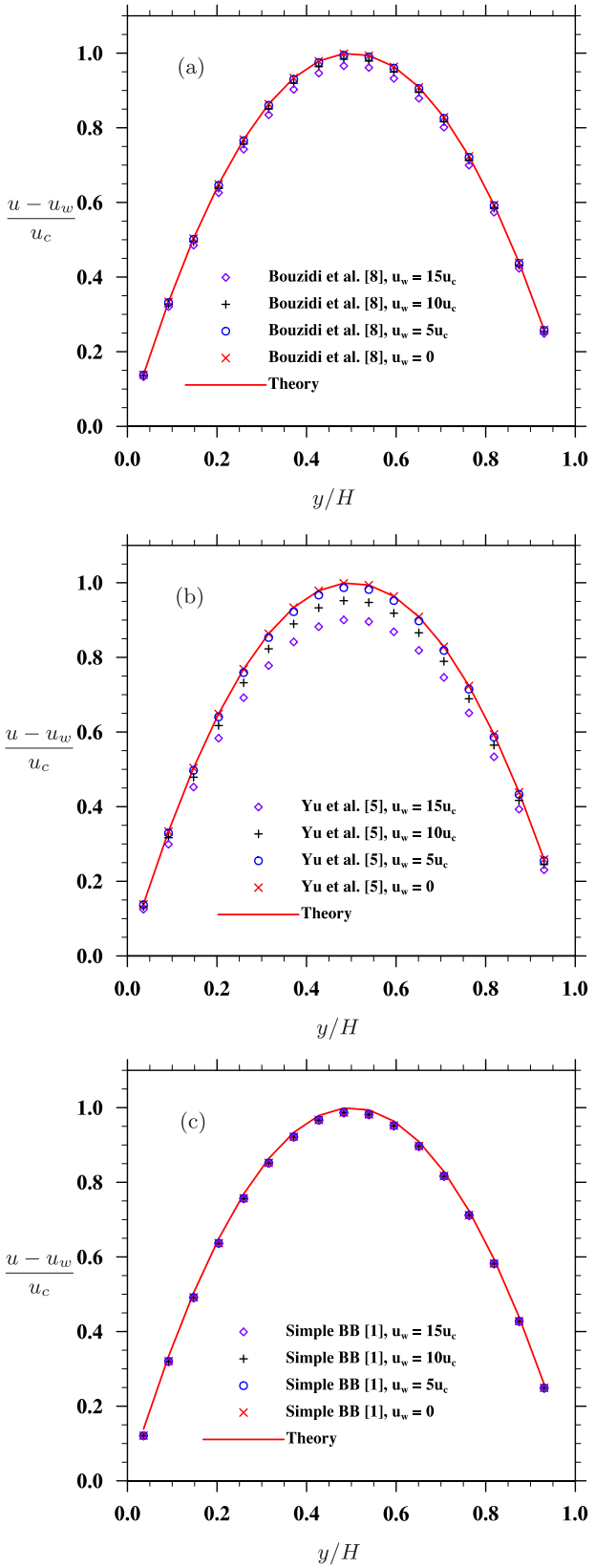

FIG. 3. The steady-state velocity profiles when different reference (moving-wall) velocities are applied: (a) with Bouzidi *et al.*'s [8] bounce-back scheme, (b) with Yu *et al.*'s [5] bounce-back scheme, and (c) with a simple bounce-back scheme [1].

In Table I, we calculate the $L1$ and $L2$ error norms of the velocity, which are defined as

$$\varepsilon_{L1} = \frac{\sum_{\mathbf{x}} |u_n(\mathbf{x}) - u_t(\mathbf{x})|}{\sum_{\mathbf{x}} |u_t(\mathbf{x})|}, \tag{23a}$$

$$\varepsilon_{L2} = \frac{\sqrt{\sum_{\mathbf{x}} |u_n(\mathbf{x}) - u_t(\mathbf{x})|^2}}{\sqrt{\sum_{\mathbf{x}} |u_t(\mathbf{x})|^2}}, \tag{23b}$$

where u_n and u_t are the numerical and theoretical streamwise velocity, respectively. When the wall velocity is large, the VGI error severely affects the accuracy of LBM simulation when the interpolated bounce-back schemes are used. According to our previous analysis in Eq. (20), the magnitude of the VGI error is expected to be on the order of $O(u_w^2)$. In Table I, the $L1$ and $L2$ error norms shown in the parentheses are those minus the corresponding error with $u_w = 0$ and then normalized by $(u_w/u_c)^2$. Indeed, in each case, it is confirmed that the VGI error scales with u_w^2. This feature does not apply very well for the simple bounce-back case. For the simple bounce-back scheme, the numerical errors are mainly contributed by its intrinsic first-order accuracy. The $L1$ and $L2$ norms only have a weak dependence on the reference wall velocity.

Figure 4 shows the total hydrodynamic force $\mathbf{F}$ acting on the two walls with five momentum exchange schemes, i.e., the conventional momentum exchange method, and four modified schemes by Caiazzo and Junk [12], Clausen and Aidun [13], Chen *et al.* [14], and Wen *et al.* [15], respectively. The black straight line indicates the total driving force $\mathbf{G}$ applied to the system. When the flow reaches a steady state, the total driving force should be balanced with the total drag $\mathbf{F}'$ exerted by the walls, i.e., $\mathbf{G} + \mathbf{F}' = \mathbf{0}$. Additionally, Newton's Third Law requires that the hydrodynamic force acting on the wall and the drag force acting on the fluid be equal and opposite, $\mathbf{F} = -\mathbf{F}'$, which yields $\mathbf{G} = \mathbf{F}$.

With both bounce-back schemes, Wen *et al.*'s [15] one-sided correction fails to satisfy Newton's Third Law. The breakdown of Newton's Third Law originates from the imbalance between Eqs. (18) and (8). On the other hand, the correction terms in Refs. [12–14] vanish due to the fact that both corrections are independent of the local flow and mesoscopic distributions. More specifically, here $\mathbf{u}_w \cdot \mathbf{n} = \mathbf{0}$, thus Clausen and Aidun's [13] correction is then zero. Caiazzo and Junk's [12] and Chen *et al.*'s [14] corrections are also zero in this case because the link configurations for the top and bottom walls are mirrored. Although the distribution functions at a boundary node near the top wall may be different from the distribution functions at a boundary node near the bottom wall, both Caiazzo and Junk's and Chen *et al.*'s correction terms are not affected by such a difference. Therefore, the schemes of Caiazzo and Junk, Clausen and Aidun, and Chen *et al.* maintain Newton's Third Law in this case. Wen *et al.*'s correction term, however, is affected by this difference in the distribution functions. Thus Wen *et al.*'s scheme violates Newton's Third Law in this case.

TABLE I. The $L1$ and $L2$ errors for the simulated steady-state velocity field with different bounce-back schemes, using various reference velocities.

u_w/u_0	Ref. [8], ε_{L1}	Ref. [8], ε_{L2}	Ref. [5], ε_{L1}	Ref. [5], ε_{L2}	Simple BB [1], ε_{L1}	Simple BB [1], ε_{L2}
0	8.194×10^{-4}	7.528×10^{-4}	6.828×10^{-4}	6.279×10^{-4}	1.760×10^{-2}	1.618×10^{-2}
5	$4.552 \times 10^{-3}(1.493 \times 10^{-4})$	$4.375 \times 10^{-3}(1.449 \times 10^{-4})$	$1.264 \times 10^{-2}(4.783 \times 10^{-4})$	$1.241 \times 10^{-2}(4.713 \times 10^{-4})$	$1.804 \times 10^{-2}(1.760 \times 10^{-5})$	$1.658 \times 10^{-2}(1.600 \times 10^{-5})$
10	$1.600 \times 10^{-2}(1.518 \times 10^{-4})$	$1.565 \times 10^{-2}(1.490 \times 10^{-4})$	$4.815 \times 10^{-2}(4.747 \times 10^{-4})$	$4.770 \times 10^{-2}(4.707 \times 10^{-4})$	$1.916 \times 10^{-2}(1.560 \times 10^{-5})$	$1.761 \times 10^{-2}(1.430 \times 10^{-5})$
15	$3.419 \times 10^{-2}(1.483 \times 10^{-4})$	$3.363 \times 10^{-2}(1.461 \times 10^{-4})$	$1.005 \times 10^{-1}(4.436 \times 10^{-4})$	$9.984 \times 10^{-2}(4.409 \times 10^{-4})$	$2.056 \times 10^{-2}(1.316 \times 10^{-5})$	$1.890 \times 10^{-2}(1.209 \times 10^{-5})$

III. A BOUNCE-BACK SCHEME BASED ON COORDINATE TRANSFORMATION

In the previous section, we analyzed the origin of VGI errors for both the solid and fluid phases, along with the

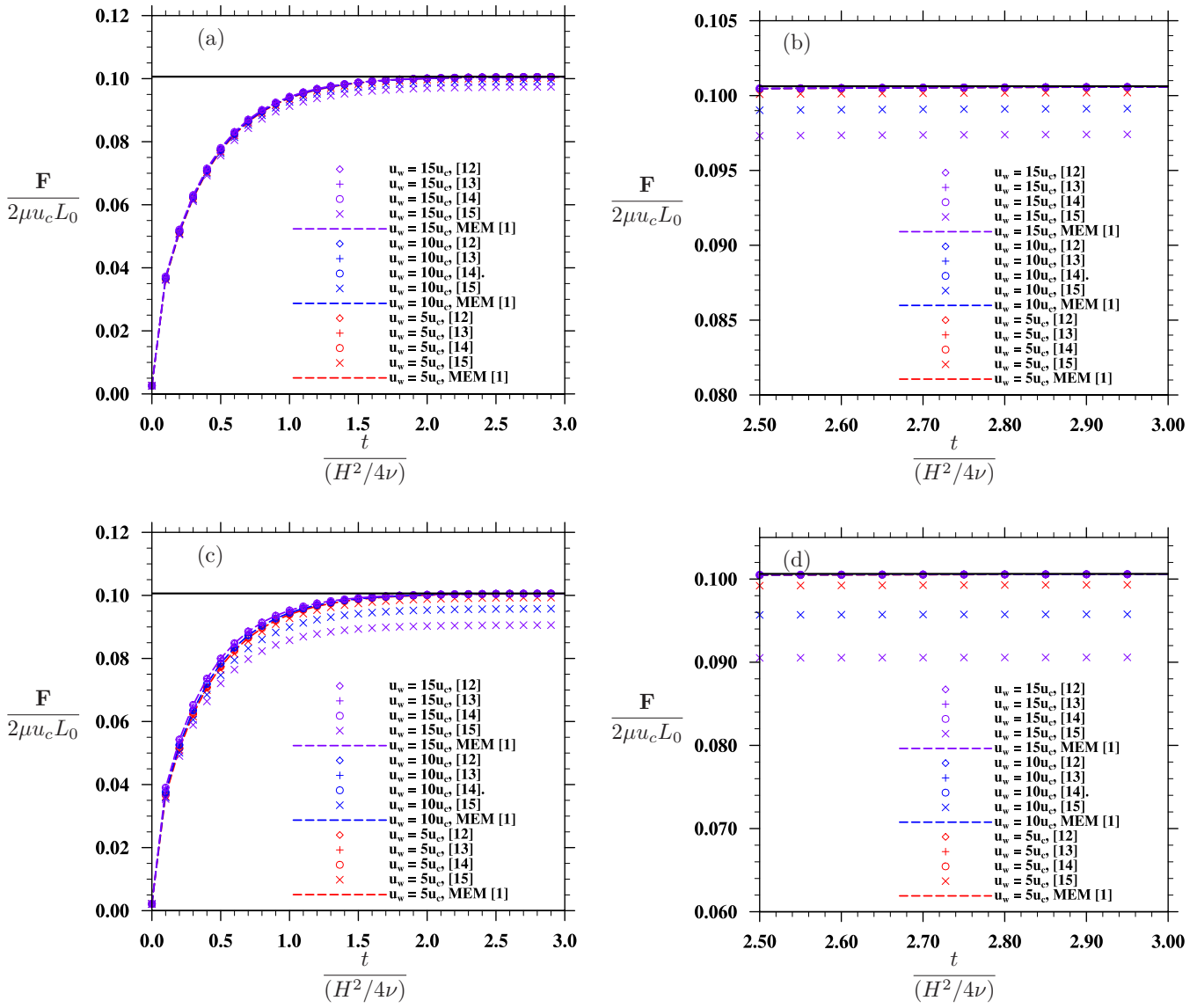

FIG. 4. The time-dependent total hydrodynamic force acting on the two walls calculated with different momentum exchange schemes: (a) with Bouzidi *et al.*'s [8] bounce-back scheme; (b) zoom-in plot of (a); (c) with Yu *et al.*'s [5] bounce-back scheme; and (d) zoom-in plot of (c). $L_0 = \sqrt{h^2 + L^2}$.

previous efforts to restore Galilean invariance on the solid phase. Without a simultaneous correction to the fluid phase, the previous efforts are deemed incomplete. The correction on the fluid phase depends entirely on the details of the bounce-back scheme. When the solid boundary undergoes shifting relative to the lattice nodes, a self-healing mechanism can be triggered, as explained in Sec. II C. Although the correction of hydrodynamic force evaluation on the solid phase and the self-healing mechanism on the fluid phase together may not satisfy either Galilean invariance or Newton's Third Law at each step, they seem to work well when integrated over time, as indicated by the reasonable results of particle dynamics in the previous simulations of turbulent particle-laden flow [14,15,24,25]. The VGI error on the fluid phase does emerge when the moving solid boundary is stationary relative to the lattice nodes, and when the self-healing mechanism for the VGI error in the fluid phase is not present. Since the boundary force exerted on the fluid is intrinsically determined by Eq. (8), where the only degree of freedom is the bounce-back population $f_{\bar{i}}$, to restore the Galilean invariance we need to design better boundary schemes.

In this paper, we present a bounce-back scheme to remove the VGI error when the moving boundary is stationary relative to the lattice nodes, i.e., when the node-type switching is absent. Our basic idea is to replace the bounce-back that occurs in a frame fixed to lattice nodes to a bounce-back implementation in a frame moving with the wall. This ensures that the bounce-back is always performed in a transformed frame where the wall is static. To achieve this, the distribution functions on the boundary nodes in the transformed frame need to be constructed. In the LBM, we can always partition the distribution function f_i into two parts: the equilibrium part $f_i^{(\mathrm{eq})}$ and the nonequilibrium part $f_i^{(\mathrm{neq})}$. The equilibrium part contains information on the conserved quantities (density,

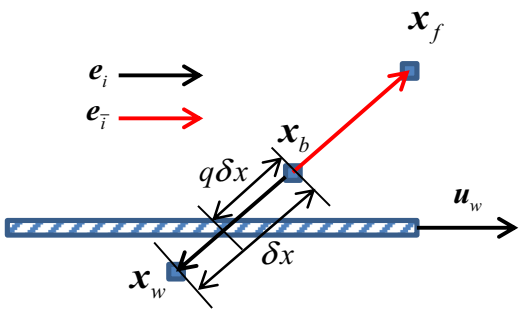

FIG. 5. Sketch of a boundary node that interacts with a moving wall, used to illustrate our proposed bounce-back implementation.

momentum) and thus can be calculated directly from the conserved quantities that are known in both frames of reference. On the other hand, the nonequilibrium part contains information on the nonconserved quantities (stress, energy flux, etc.), which in general can be approximated as functions of only strain rates [21]. Therefore, the nonequilibrium part is not affected by the constant frame velocity or the VGI error. Thus based on this understanding of the LBM, we can transform distribution functions between a static frame and a moving frame of reference.

For a boundary configuration shown in Fig. 5, our proposed bounce-back implementation consists of the following steps:

(i) After the collision substep, starting with the distribution functions in the *fixed* coordinate system (i.e., the coordinate system attached to the lattice grid), we construct the distribution functions in the coordinate system moving with the wall (the *moving* coordinate system) for *all* distribution functions that reach the boundary fluid node $\mathbf{x}_b$ after propagation. These distribution functions include two sets, namely the distribution functions that arrive at $\mathbf{x}_b$ from direct propagation (including the one at rest) and those from bounce-back. For the first group, we have

$$f_i'(t+\delta_t,\mathbf{x}_b) = f_i'^{*}(t,\mathbf{x}_b-\mathbf{e}_i), \tag{24}$$

where f with a superscript prime indicates the distribution functions in the *moving* coordinate system, while $*$ indicates the postcollision distribution functions. For the second set of distribution functions, a certain bounce-back scheme is applied. Note that the scheme could be any bounce-back scheme per the user's own choice. For demonstration purposes, we use the double linear interpolation scheme proposed by Yu *et al.* [5],

$$f_{\bar{i}}'(t+\delta_t,\mathbf{x}_b) = \frac{q}{1+q} f_i'^{*}(t,\mathbf{x}_b) + \frac{1-q}{1+q} f_i'^{*}(t,\mathbf{x}_f) + \frac{q}{1+q} f_{\bar{i}}'^{*}(t,\mathbf{x}_b). \tag{25}$$

All the involving postcollision distribution functions in the *moving* coordinate system are transformed from the *fixed* coordinate system as

$$f_i'^{*}(t,\mathbf{x}) = f_i^{(\mathrm{neq}),*}(t,\mathbf{x};\mathbf{u}^*,\delta\rho^*) + f_i^{(\mathrm{eq}),*}(t,\mathbf{x};\mathbf{u}^*-\mathbf{u}_w,\delta\rho^*), \tag{26}$$

where $\mathbf{u}^*$ and $\delta\rho^*$ are the postcollision local velocity and density fluctuation at the location $\mathbf{x}$.

(ii) Next, use $f_i'(t+\delta_t,\mathbf{x}_b)$ to update the density fluctuation and velocity at $\mathbf{x}_b$ in the *moving* coordinate system,

$$\delta\rho'(t+\delta_t,\mathbf{x}_b) = \sum_i f_i'(t+\delta_t,\mathbf{x}_b), \quad \rho_0\mathbf{u}'(t+\delta_t,\mathbf{x}_b) = \sum_i f_i'(t+\delta_t,\mathbf{x}_b)\mathbf{e}_i. \tag{27}$$

(iii) Finally, transform *all* distribution functions at $\mathbf{x}_b$ in the *moving* coordinate system back to the *fixed* coordinate system as

$$f_i(t+\delta_t,\mathbf{x}_b) = f_i'^{(\mathrm{eq})}(t+\delta_t,\mathbf{x}_b;\mathbf{u}'+\mathbf{u}_w,\delta\rho') + f_i'^{(\mathrm{neq})}(t+\delta_t,\mathbf{x}_b;\mathbf{u}',\delta\rho'). \tag{28}$$

Since in step (iii) *all* distribution functions are updated, the momentum exchange between solid and fluid phases at a boundary node obviously contains two parts. The first part is realized via momentum exchange during the bounce-back. At the same time, the momentum carried by the direct streaming from the neighboring nodes could also have been modified. This part of the momentum change should be taken into consideration in order to obey Newton's Third Law *locally*. In summary, the hydrodynamic force acting on the solid surface should be calculated as

$$\mathbf{F}(\mathbf{x}_b,t)\delta_t = \sum_{\mathrm{Blinks}} [f_{\bar{i}}(t+\delta_t,\mathbf{x}_b) + f_i^*(t,\mathbf{x}_b)]\mathbf{e}_i + \sum_{\mathrm{others}} [f_i(t+\delta_t,\mathbf{x}_b) - f_i^*(t,\mathbf{x}_b-\mathbf{e}_i\delta_t)]\mathbf{e}_i, \tag{29}$$

where the first summation is over the boundary links, while the second summation is over the remaining links at $\mathbf{x}_b$.

A few comments can be made regarding the proposed bounce-back scheme. First, it can be applied to any existing bounce-back scheme. Although we illustrate our method with Yu *et al.*'s [5] interpolated bounce-back scheme, the same process can be applied to other bounce-back schemes. Second, this bounce-back implementation should *not* be considered as a universal solution for all cases with moving boundaries. When node-type switching exists (e.g., in a solid-particle suspension), the self-healing mechanism will automatically take care of the VGI error for the moving boundaries, thus this proposed bounce-back scheme is arguably unnecessary. Ideally, the bounce-back scheme should be designed so that it can precisely address the remaining VGI error (if any) when the self-healing mechanism exists. However, it is not possible to know the magnitude of the corrections during this process in advance, thus a universal solution is unlikely to exist. In this paper, we constrain ourselves to the cases in which the self-healing mechanism is absent. Finally, although a similar philosophy of transforming distribution functions between a fixed grid and a moving grid has already been applied in the multiblock technique [31] and the immersed boundary method [32], the present scheme still has its own advantages. A second grid set in the moving frame is unnecessary in the present bounce-back scheme. The present bounce-back scheme is only applied to boundary nodes. Furthermore, when the whole

computational domain is attached with a reference velocity, the implementation of the multiblock technique or the immersed boundary method will be much harder than the present scheme.

IV. NUMERICAL VALIDATIONS

In this section, the proposed bounce-back is examined in three test cases without node-type switching: a two-dimensional Poiseuille flow between two inclined straight walls (the same case already considered in Sec. II), a three-dimensional direct numerical simulation (DNS) of a turbulent channel flow, and a three-dimensional DNS of a turbulent pipe flow.

A. A Poiseuille flow between two inclined straight walls

First, the Poiseuille flow between two inclined straight walls, driven by a body force, is tested with the proposed bounce-back scheme. As we have demonstrated in Sec. II, due to the VGI error for the fluid phase, the resulting fluid momentum deviates significantly from the theoretical solution. The test runs utilize the same parameter settings as in Sec. II. The proposed bounce-back scheme is implemented using both Bouzidi *et al.*'s [8] and Yu *et al.*'s [5] bounce-back schemes, and the corresponding results of velocity profiles with a wall velocity $u_w = 15u_c$ at different times are presented in Fig. 6. For complete assessment, the same results based on the simple bounce-back scheme [1] are also provided in parallel.

As shown in Fig. 6, when the interpolated bounce-back schemes are used, the velocity profiles at different times collapse well with the corresponding theoretical results, even with this largest wall velocity. This is in contrast with the large derivations in Fig. 3, which indicates that the VGI error has been significantly suppressed with the proposed bounce-back scheme. On the other hand, the velocity profiles based on the simple bounce-back scheme deviate from the theory at later times, which is mainly due to the first-order accuracy of the simple bounce-back scheme. Similar to Sec. II, the steady-state velocity profiles with different wall velocities and their error norms are presented in Fig. 7 and Table II, respectively. The values in parentheses in Table II again represent the error norms after subtracting their corresponding norms with $u_w = 0$ and then divided by $(u_w/u_c)^2$. Compared with the results in Fig. 3 and Table I, we can clearly observe that the proposed bounce-back scheme has successfully reduced the error in the velocity calculation by at least one order of magnitude when incorporating the two interpolation schemes. On the contrary, when the simple bounce-back scheme is used, the error norms become slightly larger. As we have demonstrated before, the VGI error (if it exists) is not significant with the use of the simple bounce-back scheme, which makes our correction arguably unnecessary. Furthermore, unlike the error norms shown in Table I due to VGI, for the two interpolated bounce-back schemes, the error norms in Table II no longer scale with $O(u_w^2)$, implying that the majority of the original VGI errors have been eliminated by the proposed coordinate transformation method. For the simple bounce-back case, the error norms in the parentheses still scale with $O(u_w^2)$.

The hydrodynamic force as a function of time is shown in Fig. 8 for different wall velocity magnitudes. Due to the

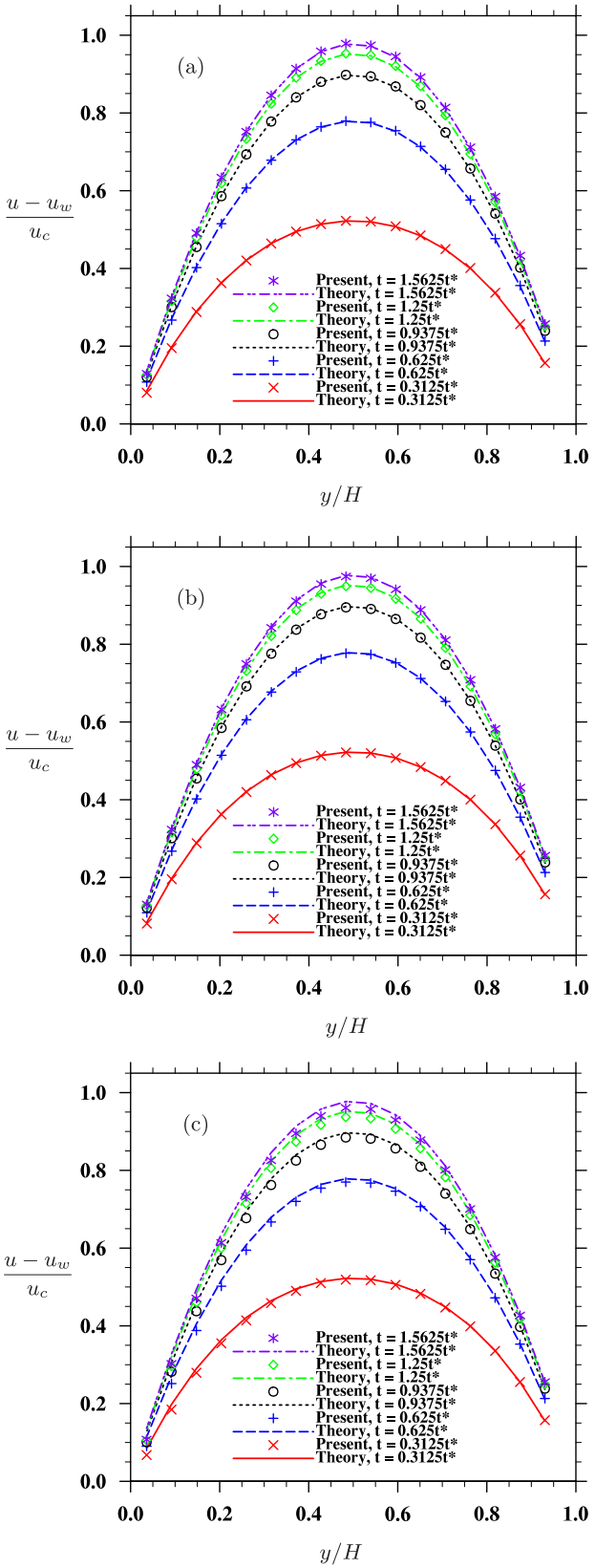

FIG. 6. The velocity profiles at different times using the proposed bounce-back scheme with $u_w = 15u_c$: (a) based on Bouzidi *et al.*'s [8] bounce-back scheme, (b) based on Yu *et al.*'s [5] bounce-back scheme, and (c) based on a simple bounce-back scheme [1]. The dimensionless time is defined as $t^* = H^2/(4\nu)$.

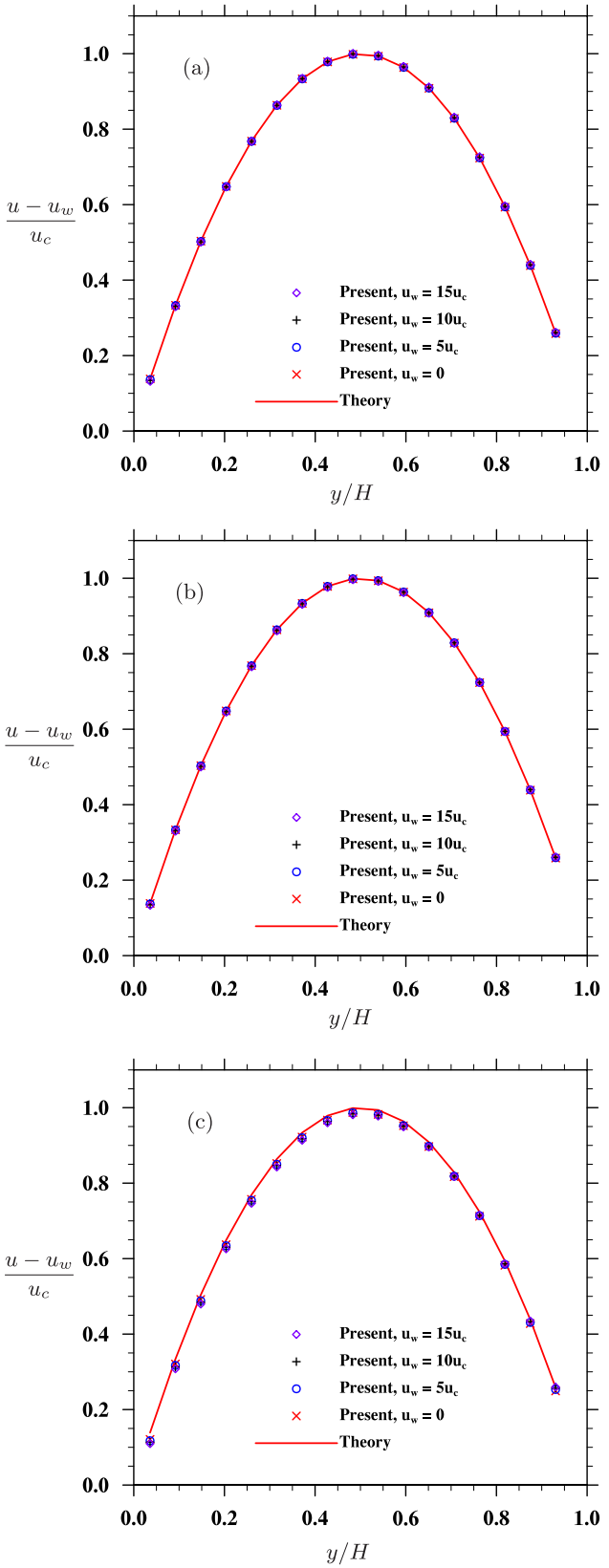

FIG. 7. The steady-state velocity profiles using the proposed bounce-back scheme with different reference velocities: (a) based on Bouzidi *et al.*'s [8] bounce-back scheme, (b) based on Yu *et al.*'s [5] bounce-back scheme, and (c) based on a simple bounce-back scheme [1].

TABLE II. The $L1$ and $L2$ errors for the simulated steady-state velocity field, using the proposed bounce-back rule incorporated with different interpolation schemes.

u_w/u_0	Ref. [8], ε_{L1}	Ref. [8], ε_{L2}	Ref. [5], ε_{L1}	Ref. [5], ε_{L2}	Simple BB [1], ε_{L1}	Simple BB [1], ε_{L2}
0	8.194×10^{-4}	7.528×10^{-4}	6.828×10^{-4}	6.279×10^{-4}	1.763×10^{-2}	1.621×10^{-2}
5	$9.440 \times 10^{-4}(4.984 \times 10^{-6})$	$1.137 \times 10^{-3}(1.539 \times 10^{-5})$	$8.000 \times 10^{-4}(4.688 \times 10^{-6})$	$8.971 \times 10^{-4}(1.077 \times 10^{-5})$	$1.833 \times 10^{-2}(2.800 \times 10^{-5})$	$1.714 \times 10^{-2}(3.720 \times 10^{-5})$
10	$1.888 \times 10^{-3}(1.069 \times 10^{-5})$	$2.091 \times 10^{-3}(1.338 \times 10^{-5})$	$1.848 \times 10^{-3}(1.165 \times 10^{-5})$	$1.974 \times 10^{-3}(1.346 \times 10^{-5})$	$2.038 \times 10^{-2}(2.750 \times 10^{-5})$	$1.974 \times 10^{-2}(3.530 \times 10^{-5})$
15	$3.539 \times 10^{-3}(1.209 \times 10^{-5})$	$3.658 \times 10^{-3}(1.291 \times 10^{-5})$	$3.857 \times 10^{-3}(1.411 \times 10^{-5})$	$3.935 \times 10^{-3}(1.470 \times 10^{-5})$	$2.367 \times 10^{-2}(2.684 \times 10^{-5})$	$2.363 \times 10^{-2}(3.298 \times 10^{-5})$

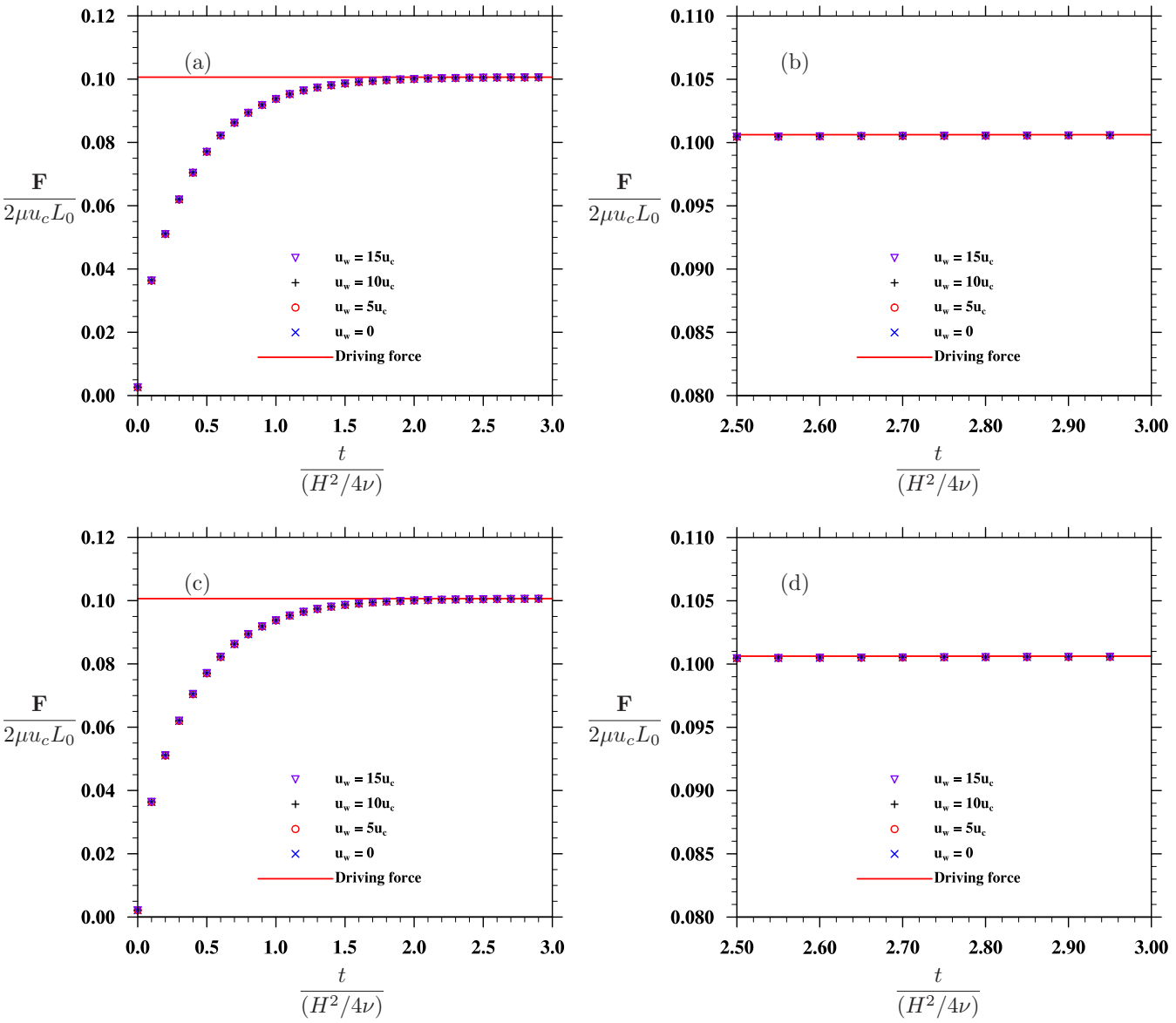

FIG. 8. The time-dependent total hydrodynamic force acting on the two walls with different wall velocities using the proposed bounce-back scheme: (a) based on Bouzidi *et al.*'s [8] bounce-back scheme; (b) zoom-in plot of (a); (c) based on Yu *et al.*'s [5] bounce-back scheme; and (d) zoom-in plot of (c). $L_0 = \sqrt{h^2 + L^2}$.

consideration of the Newton's Third Law in the proposed method, the hydrodynamic force is clearly equal to the driving force when the flow reaches steady state, as indicated in Fig. 8, for all wall velocity magnitudes tested.

B. Direct numerical simulation of a turbulent channel flow

Next, we apply our proposed bounce-back scheme in direct numerical simulation of fully developed turbulent channel flow. For a boundary node $\mathbf{x}_b$ near a straight channel wall, as shown in Fig. 9, the nodewise VGI error depends on the bounce-back scheme being used. When the midlink bounce-back is applied, although a certain VGI error is carried by the bounce-back on a single link i, it cancels precisely with the corresponding VGI error carried by link j, as one can prove from Eq. (13). The straight wall guarantees the coexistence of links i and j. When an interpolated bounce-back is used, on the other hand, the VGI error carried by a single link not only depends on the information at the boundary node $\mathbf{x}_b$, but also on the extensional node(s) used in the interpolation. Due to the

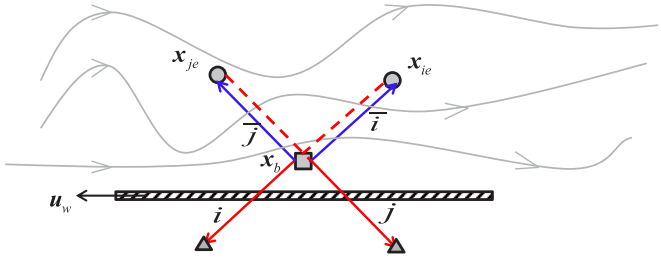

FIG. 9. A sketch of boundary configuration in a turbulent channel flow.

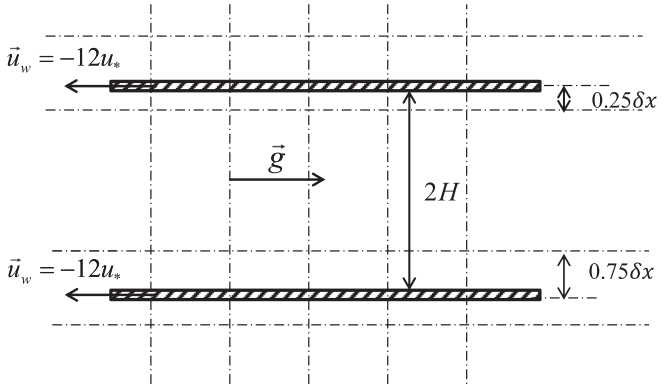

FIG. 10. Grid arrangement in the turbulent channel flow simulation.

high nonuniformity in the turbulent flow, the information at the two extensional nodes ie and je is unequal, which prevents the VGI errors from precise cancellation. Therefore, the VGI errors may affect the overall results.

Based on the above analysis, our simulation is carried out with the interpolated bounce-back. The channel center is purposely shifted by 0.25 lattice spacing to create the need to use an interpolated bounce-back to maintain overall second-order accuracy, as shown in Fig. 10. A nonzero wall velocity $u_w = -12u_*$ that is opposite to the driving force direction is added to both walls, where $u_* = \sqrt{\tau_w/\rho}$ is the friction velocity, τ_w is the wall shear stress (per unit area), and ρ is the fluid density. The interpolated bounce-back scheme of Yu *et al.* [5] and the corresponding new bounce-back scheme based on the same interpolation strategy are applied to handle the no-slip boundary on the walls. Other than that, the simulation parameters, the specific model parameters, the initial condition, as well as the method to excite the transition to turbulence are all identical to the "MRT" case as reported in [33].

It is noteworthy that in the direct numerical simulations of high Reynolds number flows, adding a nonzero velocity to the whole system brings a desired benefit of enhancing the numerical stability. For example, with the same simulation setup, removing the wall velocity can cause severe checkerboard instability in the channel center region, which eventually ruins the simulation, as indicated by the pressure contours in Fig. 11. At present, we are still unsure as to what exactly triggers the checkerboard instability, but such instability is only observed when the maximum (Ma) of the flow reaches a certain threshold. For channel flow where the Ma is dominated by the mean velocity in the streamwise direction, we can reduce the Ma at the channel center by adding an opposite velocity ($u_w = -12u_*$ as applied in our simulation) to the system. After adding this constant translation to the system, the simulations with both bounce-back rules are stable.

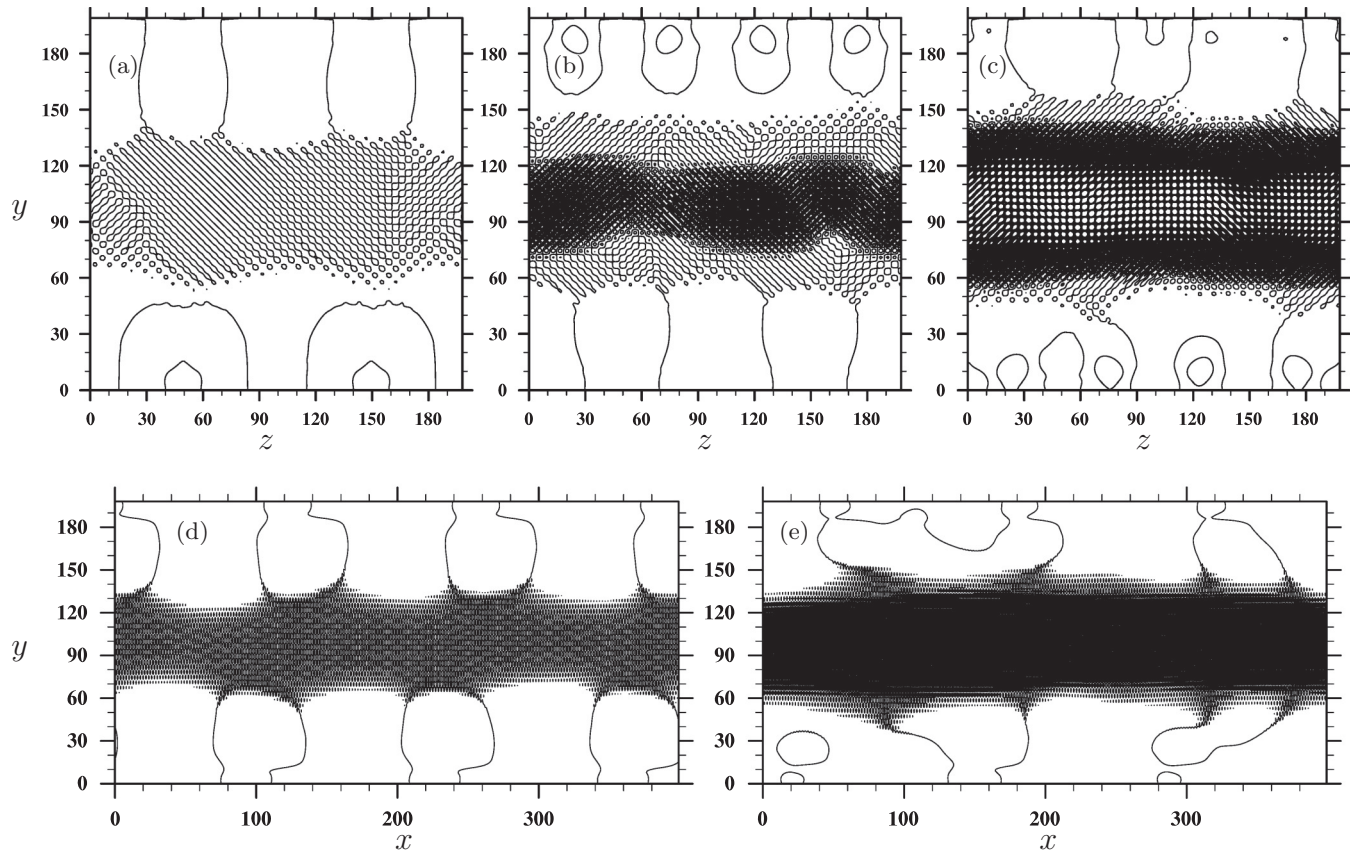

FIG. 11. Pressure contours in a turbulent channel flow simulation indicating the existence of checkerboard instability. Top row: pressure contours at a streamwise location $x = nx/2$ at (a) $t = 7000$, (b) $t = 7500$, and (c) $t = 8000$. Bottom row: pressure contours at a spanwise location $z = nz/2$ at (d) $t = 7000$ and (e) $t = 8000$.

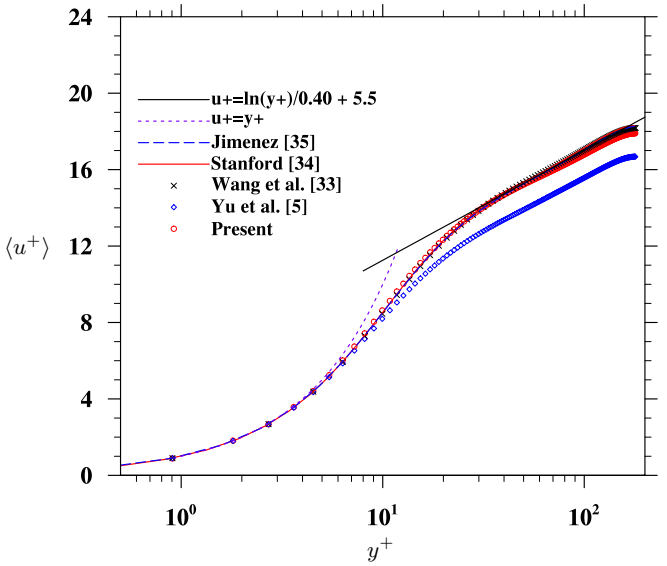

FIG. 12. The averaged mean velocity profiles at the stationary stage in the turbulent channel flow simulation.

Here we only discuss the average profiles when the flow becomes statistically stationary. The mean velocity profiles on a log-linear plot with both bounce-back rules are presented in Fig. 12. To benchmark these profiles, two profiles from pseudospectral simulations, denoted by "Stanford" [34] and "Jimenez" [35], as well as our earlier result [33] (denoted by "Wang *et al.*") based on midlink bounce-back with the same grid resolution, are also shown in the same plot. Except for the small difference exhibited near the channel center, the profile from the proposed bounce-back scheme matches perfectly with the pseudospectral results in most of the region. The small deviation at the channel center may be due to the slight asymmetry in the current simulation or the additional dissipation caused by the interpolation compared to the midlink bounce-back in our earlier study [33]. On the other hand, the mean velocity profile from Yu *et al.*'s original bounce-back deviates significantly from the benchmark results due to the VGI errors that originated from the boundary. This comparison for the more complex nonuniform unsteady flow clearly indicates that the lack of Galilean invariance in the usual bounce-back schemes can lead to erroneous results, and our proposed implementation can fix this problem.

Figures 13 and 14 show the Reynolds stress profiles and the root-mean-square (rms) velocity profiles, respectively. Compared to the mean flow property, the impact of the VGI errors on the velocity fluctuation is relatively small. This might be explained by the fact that the velocity fluctuations in a turbulent flow are more directly associated with the stress components, which are less affected by the VGI errors. Even so, a slight improvement is still observed in the Reynolds stress profiles with the proposed bounce-back scheme when compared with results from Yu *et al.*'s [5] original interpolated bounce-back scheme. The rms velocity profiles confirm that the results from our proposed bounce-back scheme match better with our earlier LBM results, which are free from the VGI errors due to use of the midlink bounce-back compared to Yu *et al.*'s original scheme.

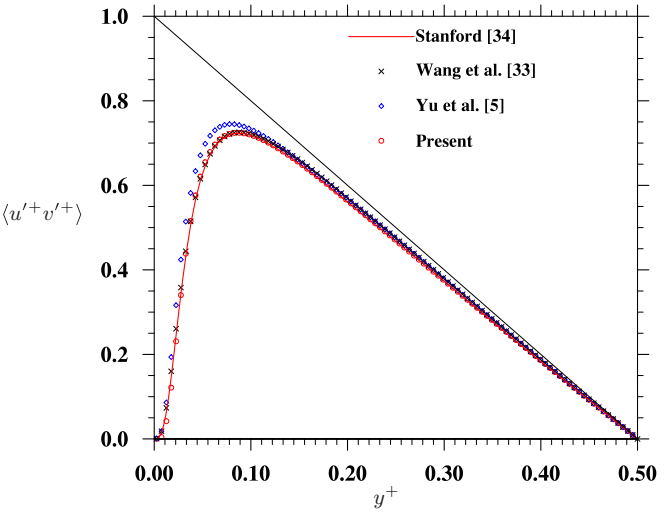

FIG. 13. The averaged Reynolds stress profiles at the stationary stage in the turbulent channel flow simulation.

Finally, at the stationary stage, we calculate the hydrodynamic force on the two walls, normalized by the total driving force. For Yu *et al.*'s bounce-back scheme, the hydrodynamic force is evaluated based on both the conventional MEM [Eq. (9)] and the GIMEM [Eq. (18)] by Wen *et al.* [15], while for our proposed bounce-back scheme, the force is calculated using Eq. (29). At the stationary stage, the average hydrodynamic force is again expected to be equal to the total driving force. As shown in Fig. 15, in this case, due to the fact that all boundary nodes have the same set of symmetric boundary links, the correction term in the GIMEM is essentially zero. As a result, the MEM and the GIMEM give identical total hydrodynamic forces when Yu *et al.*'s bounce-back scheme is used. In more general cases, for example, with curved boundaries, the GIMEM may create a nonzero correction term that leads to the breakdown of Newton's Third Law, as we demonstrated in the case of viscous flow

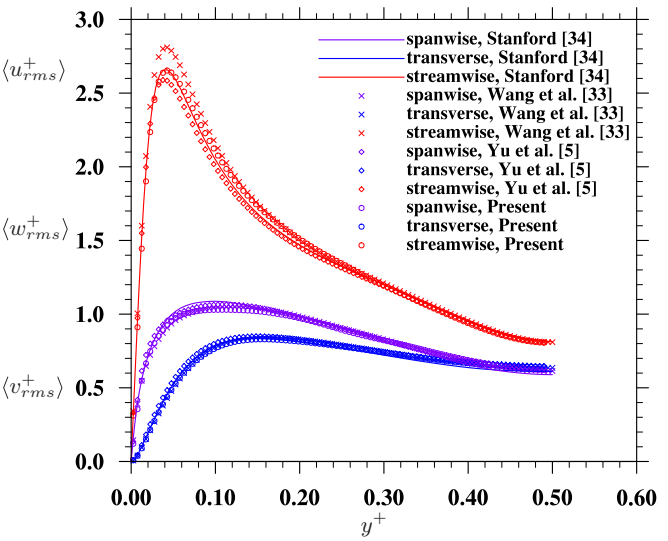

FIG. 14. The averaged rms velocity profiles at the stationary stage in the turbulent channel flow simulation.

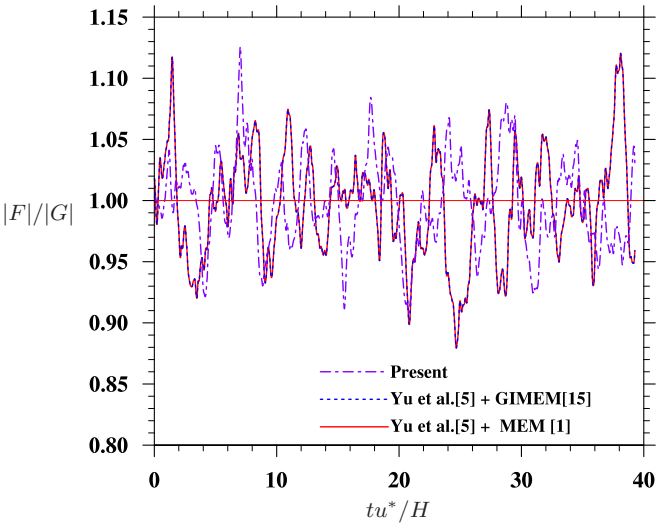

FIG. 15. The normalized total hydrodynamic force acting on the two walls at stationary state in the turbulent channel flow.

in the inclined channel. We will also confirm such a statement in the next section with a direct numerical simulation of turbulent pipe flow. On the other hand, the hydrodynamic force calculation in our proposed bounce-back scheme always satisfies Newton's Third Law, as confirmed by the results shown in Fig. 15. The time-averaged values of the ratio of total hydrodynamic force to total driving force are 0.9962 and 0.9975 for Yu *et al.*'s original bounce-back scheme and our proposed bounce-back scheme, respectively.

It is worth pointing out that although our proposed bounce-back scheme appears to be much more complicated than its corresponding original bounce-back rule, with careful implementation the computational overhead is negligible since the transformation is done on boundary nodes, which takes only a small portion of the whole domain. In the case of DNS of turbulent channel flow, we use two-dimensional domain decomposition to divide the whole computational domain into 200 subdomains; the time overhead of our bounce-back scheme is only 1.1% (measured by wall clock time based on two runs submitted on the same date and finished at about the same time).

C. Direct numerical simulation of a turbulent pipe flow

As a final demonstration, our proposed bounce-back scheme is also examined in our recent direct numerical simulation of a fully developed turbulent pipe flow. For a similar reason to that demonstrated in Sec. IV B, the VGI error carried by each link cannot be canceled out precisely to restore the overall GI on boundary nodes due to the use of the previous interpolated bounce-back schemes, which ensures second-order accuracy on the boundary treatment. As shown in Fig. 16, the flow in the circular pipe is driven by a constant body force ρg (per unit volume) that maintains a friction Reynolds number $\mathrm{Re}_\tau = u_* R/\nu = 180$. Again, a negative (opposite to the driving force direction) wall velocity $u_w = -12u_*$ is added to the pipe wall so the flow speed at the pipe center can be reduced in order to achieve better numerical stability, which was the initial motivation for our development in this paper.

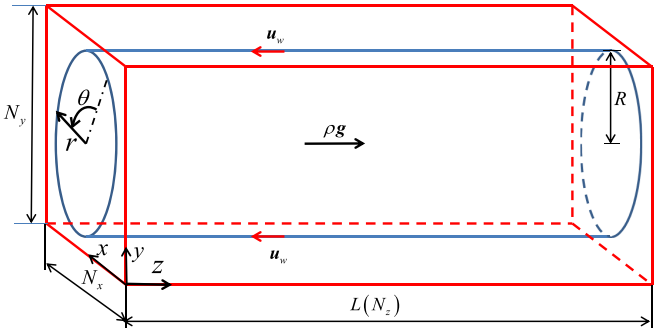

FIG. 16. Sketch of the turbulent pipe flow simulation.

On the pipe surface, the interpolated bounce-back scheme of Yu *et al.* [5] and its corresponding bounce-back scheme with the same interpolation strategy are tested.

The mean flow velocity profiles of both bounce-back schemes are presented in Fig. 17 when the flow becomes stationary. Here we use the spectral simulations done by Loulou *et al.* [36] with the friction Reynolds number $\mathrm{Re}_\tau = 190$ as the benchmark. Although this Re_τ is slightly different from the one in our simulations, its impact on the turbulent statistics is expected to be insignificant. As in the turbulent channel flow case, the mean velocity profile with Yu *et al.*'s original bounce-back scheme deviates from the spectral result significantly due to the additional drag caused by the VGI error. On the other hand, our proposed bounce-back scheme successfully eliminates the VGI error and results in a velocity profile that is in excellent agreement with the benchmark. The rms velocity profiles at the stationary stage are shown in Fig. 18. Again, as in the turbulent channel flow case, the VGI error only has a minor effect on the rms velocities in the turbulent pipe flow. This makes sense since the rms velocities measure the intensity of the velocity fluctuation, which is

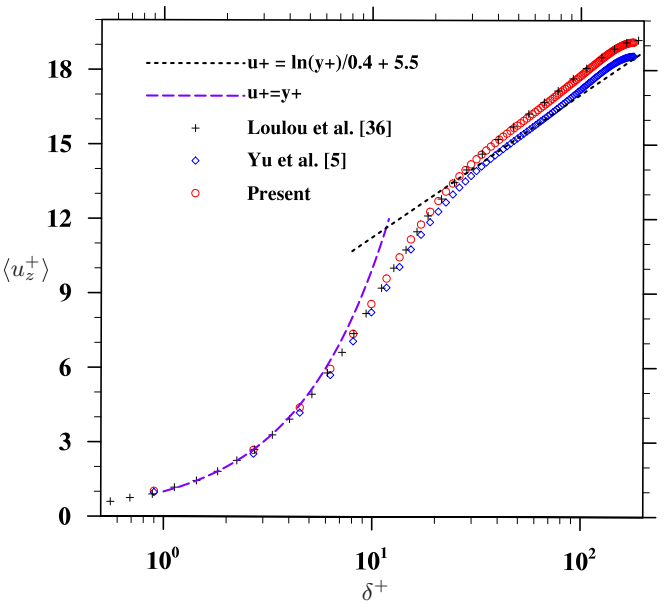

FIG. 17. The averaged mean velocity profiles at the stationary stage, relative to the pipe wall, in the turbulent pipe flow simulation.

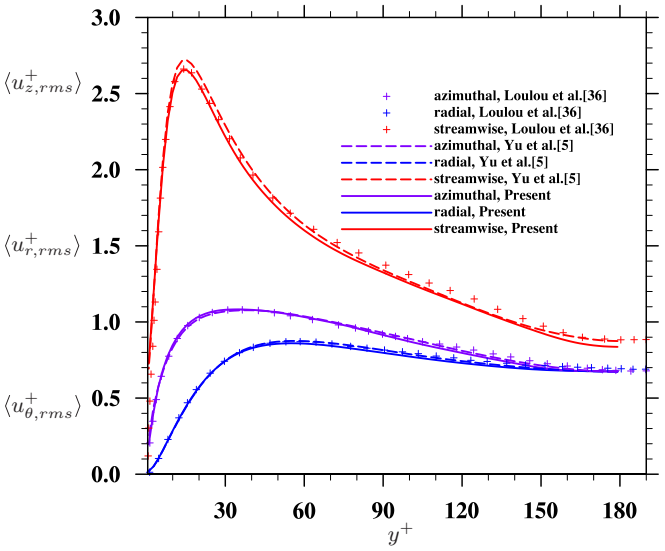

FIG. 18. The averaged rms velocity profiles at the stationary stage in the turbulent pipe flow simulation.

independent of the reference frame that we chose. Finally, we examine the hydrodynamic force evaluation at the stationary state to check if the equality between the total driving force and the total hydrodynamic force is well captured, as is required by Newton's Third Law. Clearly, as shown in Fig. 19, when Yu *et al.*'s bounce-back scheme is used, the normalized hydrodynamic force evaluated by the MEM oscillates around unity while that calculated by the GIMEM is generally smaller than 1. This confirms our statement in Sec. IV B that the GIMEM creates nonzero corrections in more general cases, which leads to the breakdown of Newton's Third Law. Again, the force evaluation in our proposed bounce-back scheme obeys Newton's Third Law well, as the total normalized hydrodynamic force varies around unity. The time-averaged values of the normalized hydrodynamic force are 1.0004, 0.9709, and 1.0014 for the MEM and the GIMEM with Yu

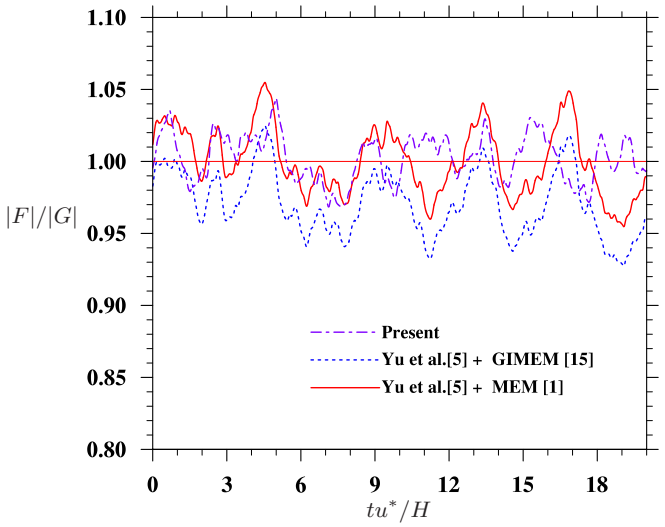

FIG. 19. The normalized total hydrodynamic force acting on the two walls at stationary state in the turbulent pipe flow.

et al.'s bounce-back scheme and our proposed bounce-back scheme, respectively.

V. CONCLUSIONS

In this work, we analyzed the problem of lacking Galilean invariance in the momentum exchange between solid and fluid phases when previous bounce-back schemes and a momentum exchange method were used. We stressed the need to consider Galilean invariance for both the hydrodynamic force acting on the solid surface and the momentum exchange of the fluid phase due to the fluid-moving wall interaction, as a requirement from Newton's Third Law.

Specifically, the main conclusions of this study are summarized as follows:

(i) The lack of Galilean invariance in the force evaluation based on the momentum exchange method has been widely recognized in recent years. Different modified momentum exchange schemes are proposed to eliminate the violation of Galilean invariance (VGI) errors in force evaluation on a solid body [12–15]. However, as required by Newton's Third Law, a corresponding error also exists in the fluid phase. The error in the fluid phase is purely due to the inappropriate construction of the missing distribution functions on a boundary node, which has not been addressed in previous studies.

(ii) In the LBM simulations involving solid-fluid interactions, the impulsive momentum exchange occurs between the two phases, taking place when a solid node being uncovered or a fluid node being covered can be viewed as an automatic correction to the VGI error in the fluid phase. However, in the cases without such a self-healing mechanism, the VGI error in the fluid phase is intact and can cause severe inaccuracy in the fluid velocity calculations. Furthermore, the one-sided correction of the VGI error on the solid surface, without a simultaneous correction on the fluid phase, could violate Newton's Third Law under certain circumstances. These problems have been demonstrated using LBM simulations of viscous flow in an inclined channel when a significant translational velocity (u_w) is added to the whole system; in this case, we show that the VGI error is proportional to u_w^2. Clearly, this can ruin the default accuracy of the LBM, which is know to have an inherent truncation error of $O(u^3)$.

(iii) A bounce-back scheme based on the coordinate transformation is then proposed to address the VGI error in the fluid phase where the node-type switching is absent. In this scheme, the distribution functions at the boundary nodes are transformed from a fixed coordinate system to a moving coordinate system before the bounce-back is implemented. Then, the post bounce-back distribution functions at the boundary nodes are transformed back to the fixed coordinate system. This coordinate transformation treatment can be easily combined with the existing interpolated bounce-back schemes to maintain the desired accuracy of the LBM simulations. The force evaluation method is also modified to satisfy Newton's Third Law.

(iv) The new bounce-back scheme is tested in three benchmark cases: a Poiseuille flow between two inclined straight walls, a turbulent channel flow, and finally a turbulent pipe flow. Compared with the existing bounce-back schemes,

our proposed bounce-back scheme can significantly improve the accuracy of the simulated flow velocity in both laminar and turbulent flows.

(v) The additional computational cost brought about by the use of our proposed bounce-back scheme compared with the original scheme is negligibly small, typically only around 1%.

It is hoped that the results in this study will generate a renewed interest in revisiting rigorous implementation issues in the LBM associated with a moving curved boundary, specifically the enforcement of Galilean invariance and Newton's Third Law at the fluid-solid interface. The LBM can become a very accurate computational fluid dynamics tool if unexpected issues, such as those associated with a general moving solid surface, which are recognized and treated in this study, can be fully understood. Other methods could be developed to ensure the simultaneous Galilean invariance of the simulated force on the moving solid boundary and the resulting fluid flow.

Finally, we stress that the current study only considers the case in which the solid boundary is moving along a fixed line (in two dimensions) or a fixed surface (in three dimensions). The case of a freely moving fluid-solid surface should be reexamined. In particular, consideration of the full Galilean invariance requirement outlined in this paper may help remove the often-encountered oscillations of resulting hydrodynamic force on the solid body [24]. However, determining how to improve the implementation for that case remains an open question.

ACKNOWLEDGMENTS

This work has been supported by the U.S. National Science Foundation (NSF) under Grants No. CNS1513031, No. CBET-1235974, and No. AGS-1139743, and by Air Force Office of Scientific Research under Grant No. FA9550-13-1-0213. L.P.W. also acknowledges support from the Ministry of Education of P.R. China, and Huazhong University of Science and Technology through Chang Jiang Scholar Visiting Professorship. Computing resources are provided by National Center for Atmospheric Research through CISL-P35751014, by CISL-UDEL0001, and by the University of Delaware through NSF CRI 0958512.

[1] A. J. Ladd, Numerical simulations of particulate suspensions via a discretized Boltzmann equation. Part 1. Theoretical foundation, J. Fluid Mech. **271**, 285 (1994).

[2] C. K. Aidun, Y. Lu, and E.-J. Ding, Direct analysis of particulate suspensions with inertia using the discrete Boltzmann equation, J. Fluid Mech. **373**, 287 (1998).

[3] A. Ten Cate, J. J. Derksen, L. M. Portela, and H. E. Van Den Akker, Fully resolved simulations of colliding monodisperse spheres in forced isotropic turbulence, J. Fluid Mech. **519**, 233 (2004).

[4] H. Gao, H. Li, and L.-P. Wang, Lattice Boltzmann simulation of turbulent flow laden with finite-size particles, Comput. Math. Appl. **65**, 194 (2013).

[5] D. Yu, R. Mei, L.-S. Luo, and W. Shyy, Viscous flow computations with the method of lattice Boltzmann equation, Progr. Aerospace Sci. **39**, 329 (2003).

[6] I. Ginzburg and D. d'Humières, Multireflection boundary conditions for lattice Boltzmann models, Phys. Rev. E **68**, 066614 (2003).

[7] C. Pan, L.-S. Luo, and C. T. Miller, An evaluation of lattice Boltzmann schemes for porous medium flow simulation, Comput. Fluids **35**, 898 (2006).

[8] M. Bouzidi, M. Firdaouss, and P. Lallemand, Momentum transfer of a Boltzmann-lattice fluid with boundaries, Phys. Fluids (1994-present) **13**, 3452 (2001).

[9] R. Mei, W. Shyy, D. Yu, and L.-S. Luo, Lattice Boltzmann method for 3-d flows with curved boundary, J. Comput. Phys. **161**, 680 (2000).

[10] R. Mei, D. Yu, W. Shyy, and L.-S. Luo, Force evaluation in the lattice Boltzmann method involving curved geometry, Phys. Rev. E **65**, 041203 (2002).

[11] H. Li, H. Fang, Z. Lin, S. Xu, and S. Chen, Lattice Boltzmann simulation on particle suspensions in a two-dimensional symmetric stenotic artery, Phys. Rev. E **69**, 031919 (2004).

[12] A. Caiazzo and M. Junk, Boundary forces in lattice Boltzmann: Analysis of momentum exchange algorithm, Comput. Math. Appl. **55**, 1415 (2008).

[13] J. R. Clausen and C. K. Aidun, Galilean invariance in the lattice-Boltzmann method and its effect on the calculation of rheological properties in suspensions, Int. J. Multiphase Flow **35**, 307 (2009).

[14] Y. Chen, Q. Cai, Z. Xia, M. Wang, and S. Chen, Momentum-exchange method in lattice Boltzmann simulations of particle-fluid interactions, Phys. Rev. E **88**, 013303 (2013).

[15] B. Wen, C. Zhang, Y. Tu, C. Wang, and H. Fang, Galilean invariant fluid-solid interfacial dynamics in lattice Boltzmann simulations, J. Comput. Phys. **266**, 161 (2014).

[16] S. Krithivasan, S. Wahal, and S. Ansumali, Diffused bounce-back condition and refill algorithm for the lattice Boltzmann method, Phys. Rev. E **89**, 033313 (2014).

[17] S. Hou, Q. Zou, S. Chen, G. D. Doolen, and A. C. Cogley, Simulation of cavity flow by the lattice Boltzmann method, J. Comput. Phys. **118**, 329 (1995).

[18] M. Junk, A. Klar, and L.-S. Luo, Asymptotic analysis of the lattice Boltzmann equation, J. Comput. Phys. **210**, 676 (2005).

[19] W.-A. Yong and L.-S. Luo, Accuracy of the viscous stress in the lattice Boltzmann equation with simple boundary conditions, Phys. Rev. E **86**, 065701 (2012).

[20] P. Lallemand and L.-S. Luo, Theory of the lattice Boltzmann method: Dispersion, dissipation, isotropy, Galilean invariance, and stability, Phys. Rev. E **61**, 6546 (2000).

[21] J. Latt, B. Chopard, O. Malaspinas, M. Deville, and A. Michler, Straight velocity boundaries in the lattice Boltzmann method, Phys. Rev. E **77**, 056703 (2008).

[22] Z.-G. Feng and E. E. Michaelides, The immersed boundary-lattice Boltzmann method for solving fluid-particles interaction problems, J. Comput. Phys. **195**, 602 (2004).

[23] Y. Peng and L.-S. Luo, A comparative study of immersed-boundary and interpolated bounce-back methods in lbe, Progr. Comput. Fluid Dyn. Int. J. **8**, 156 (2008).

[24] C. Peng, Y. Teng, B. Hwang, Z. Guo, and L.-P. Wang, Implementation issues and benchmarking of lattice Boltzmann method for moving rigid particle simulations in a viscous flow, Comput. Math. Appl. **72**, 349 (2016).

[25] S. Tao, J. Hu, and Z. Guo, An investigation on momentum exchange methods and refilling algorithms for lattice Boltzmann simulation of particulate flows, Comput. Fluids **133**, 1 (2016).

[26] B. Wen, C. Zhang, and H. Fang, Hydrodynamic force evaluation by momentum exchange method in lattice Boltzmann simulations, Entropy **17**, 8240 (2015).

[27] X. He and L.-S. Luo, Lattice Boltzmann model for the incompressible Navier-Stokes equation, J. Stat. Phys. **88**, 927 (1997).

[28] H. Fang, Z. Wang, Z. Lin, and M. Liu, Lattice Boltzmann method for simulating the viscous flow in large distensible blood vessels, Phys. Rev. E **65**, 051925 (2002).

[29] P. Lallemand and L.-S. Luo, Lattice Boltzmann method for moving boundaries, J. Comput. Phys. **184**, 406 (2003).

[30] A. Caiazzo, Analysis of lattice Boltzmann nodes initialization in moving boundary problems, Progr. Comput. Fluid Dyn. Int. J. **8**, 3 (2008).

[31] R. Zhang, C. Sun, Y. Li, R. Satti, R. Shock, J. Hoch, and H. Chen, Lattice Boltzmann approach for local reference frames, Commun. Comput. Phys. **9**, 1193 (2011).

[32] M. Meldi, E. Vergnault, and P. Sagaut, An arbitrary Lagrangian-Eulerian approach for the simulation of immersed moving solids with lattice Boltzmann method, J. Comput. Phys. **235**, 182 (2013).

[33] L.-P. Wang, C. Peng, Z. Guo, and Z. Yu, Lattice Boltzmann simulation of particle-laden turbulent channel flow, Comput. Fluids **124**, 226 (2016), Special Issue for ICMMES-2014.

[34] J. Kim, P. Moin, and R. Moser, Turbulence statistics in fully developed channel flow at low Reynolds number, J. Fluid Mech. **177**, 133 (1987).

[35] J. Jimenez and S. Hoyas, Turbulent fluctuations above the buffer layer of wall-bounded flows, J. Fluid Mech. **611**, 215 (2008).

[36] P. Loulou, R. D. Moser, N. N. Mansour *et al.*, Direct numerical simulation of incompressible pipe flow using a B-spline spectral method, NASA Tech. Memo. No. 110436 (1997), https://ntrs.nasa.gov/search.jsp?R=19970011270.